

Model of a GaAs Quantum Dot Embedded in a Polymorph AlGaAs Nanowire

Daniele Baretin, Alexei V. Platonov, Alessandro Pecchia, Vladimir N. Kats, George E. Cirlin, Iliya P. Soshnikov, Alexei D. Bouravleuv, Lucien Besombes, Henri Mariette, Matthias Auf der Maur, *Member, IEEE*, and Aldo Di Carlo, *Member, IEEE*

Abstract—We report on a numerical model of quasi-1-D and quasi-0-dimensional semiconductor heterostructures. This model is strictly based on experimental structures of cylindrical nanocolumns of AlGaAs grown by molecular-beam epitaxy in the (1 1 1) direction. The nanocolumns are of 20–50 nm in diameter and 0.5–1 μm in length and contain a single GaAs quantum dot of 2 nm in thickness and 15–45 nm in diameter. Since the crystal phase of these nanowires spontaneously switches during the growth from zincblende (Zb) to wurzite (Wz) structures, we implement a continuum elastic model and an eight-band $\vec{k} \cdot \vec{p}$ model for polymorph crystal structures. The model is used to compute electromechanical fields, wave-function energies of the confined states and optical transitions. The model compares a pure Zb structure with a polymorph in which the Zb disk of GaAs is surrounded by Wz barriers and results are compared to experimental photoluminescence excitation spectra. The good agreement found between theory and features in the spectra supports the polyphorm model.

Index Terms—Nanowire (NW), polymorph materials, quantum dot (QD).

I. INTRODUCTION

SINCE the discovery of self-assembled quantum dots (QD), the field of optoelectronics has moved interest on nanoobjects of different dimension, size, and shape in the search of novel useful properties. The challenge of the QD fabrication

technology is to obtain highly homogeneous arrays with little dispersion in size, composition, and shape in order to maximize quantum efficiency of LEDs and lasers. This requirement has been solved only partially with self-organization [1] that allows to achieve a rather uniform distribution of the dot sizes with dispersion of 10% [2]. However, the technique has a number of essential ineradicable lacks. For instance, because of the presence of a wetting layer, it is impossible to reach high quantum efficiencies. Furthermore, this growth process offer little to no control over the dot size, an essential parameter in order to tune the emission wavelength.

Thanks to the fast development and improvement of control in the growing conditions of nanostructures research has moved to new solutions in nanoengineering quantum confined states. The growth of free standing semiconductor nanowires (NWs) and nanocolumns is one of the most promising solution for application in nanoelectronics [3], and nanophotonics [4], thanks to a better relaxation of the strain field that allows more freedom in combining III–V materials. The technology of manufacturing such NWs is now intensively developing [5]–[13]. These NWs can include one or several QD (or quantum disks). Modern epitaxial methods allows to control the sizes and location of NW at the nanometer scale, that favorably distinguishes such QD from planar and is very attractive for applications in optoelectronic devices.

However, GaAs/AlGaAs NWs also possess growth mechanisms that might have strong influences on their electronic properties. It is known that the crystal structure of a (1 1 1) nanowire may spontaneously switch during the growth from zinc-blende (Zb) to wurzite (Wz) phases [14]. The effect leads to a strong modification of the time resolved photoluminescence (PL) spectra in the range of the optical transitions within the barrier material [10]. Besides, in these NWs structures, the recombination time can also be altered by the surface recombination rate [11]. Similarly, it is expected that optical transitions in the QD are sensitive to the crystal phase of the dot itself and its surrounding media. For example the energy position of the ground and excited states in the QD may be influenced by the electric field originating from the crystal phase transition. To observe the effect of this transition it is necessary to make a comparison between experimental data obtained by time resolved PL and PL excitation (PLE) measurements and theoretical simulations.

The electronic structures and the variation of the fundamental gap of the Wz phase of these crystals have been only quite recently studied. Knowledge of the full band structure of these polymorph materials is fundamental in order to possibly extract parameters for tight-binding (TB) [15] and $\vec{k} \cdot \vec{p}$ [16] model calculations. However, at present time only a relative

Manuscript received November 27, 2012; revised January 13, 2013; accepted January 13, 2013. The work of D. Baretin was supported by EC through the IRSES SIMTECH (GA 246937) and the Mediterranean Institute of Fundamental Physics.

D. Baretin, M. Auf der Maur, and A. Di Carlo are with the Department of Electronics Engineering, University of Rome Tor Vergata, Rome 00133, Italy (e-mail: Daniele.Baretin@uniroma2.it; auf.der.maur@ing.uniroma2.it; aldo.dicarlo@uniroma2.it).

A. V. Platonov, G. E. Cirlin, I. P. Soshnikov, and A. D. Bouravleuv are with the A.F.Ioffe Physical-Technical Institute St. Petersburg 194021, Russia (e-mail: Alexei.platonov@mail.ioffe.ru; cirlin@beam.ioffe.ru; Ipsosh@beam.ioffe.ru; bour@mail.ioffe.ru).

A. Pecchia is with the CNR-ISMN, Monterotondo 00017, Rome, Italy, and also with University of Rome Tor Vergata, Rome 00133, Italy (e-mail: pecchia@ing.uniroma2.it).

V. N. Kats is with the A.F.Ioffe Physical-Technical Institute, St. Petersburg 194021, Russia, and also with Spin Optics Laboratory, Saint Petersburg State University, Petrodvorets, St. Petersburg 198904, Russia (e-mail: Vladimir.N.Kats@gmail.com).

L. Besombes and H. Mariette are with the CEA-CNRS Group, “Nanophysique et Semiconducteurs,” Institut Néel, Grenoble F-38054, France (e-mail: lucien.besombes@grenoble.cnrs.fr; henri.mariette@cea.fr).

Color versions of one or more of the figures in this paper are available online at <http://ieeexplore.ieee.org>.

Digital Object Identifier 10.1109/JSTQE.2013.2240657

small amount of parameters for bandstructure calculations are available in the literature.

Quasi-particle calculations of newly observed Wz polymorphs of InAs and GaAs has been reported in [17] using the GW approximation. De *et al.* have presented calculations of the bulk electronic band structures of non-nitride III–V semiconductors in the Wz phase using empirical pseudopotentials including spin-orbit coupling [18], while Jancu *et al.* have studied the electronic structure of the Wz phases of GaAs and InP using a TB model and calculate the optical properties of crystal phase QD formed by thin Zb layers inserted in a Wz-InP NW [19]. Since the Zb and Wz structures differ only by the arrangement of the second neighbors of a given atom, they used the same set of parameters for the two phases, while the atomic positions are given as input data and lattice constants are precisely determined by X-ray diffraction.

Very recently quasi-particle self-consistent GW calculations have been used to analyze the band structure of GaAs in Wz phase [20]. Here, also the Kohn–Luttinger and Rashba–Sheka–Pikus effective Hamiltonian band structure parameters of Wz GaAs have been determined from these first-principles band structure calculations.

In this study, we have simulated an AlGaAs NW with an embedded GaAs QD, considering two different cases, a pure Zb case and a polymorph Wz–Zb case, respectively. Dimensions, structural, and geometric parameters have been strictly derived from experimental data. We have implemented an eight-band $\vec{k} \cdot \vec{p}$ model [21] for bandstructure calculations, and the parameters for the Pikus–Bir Hamiltonian of the Wz materials have been derived from the correspondent Zb materials using the cubic approximation as described by Chuang *et al.* [22], while the stiffness parameters of Wz crystals have been estimated from Martin’s transformations [23], [24] using the Zb parameters.

The paper is organized as follows. In the first section, we present the experimental results that have inspired our numerical investigation. In Section III, we describe the models and the way we have derived all the parameters needed in the simulations, while all the numerical results are discussed in Section IV. Finally, we give our conclusions.

II. EXPERIMENT

In these studies, we have considered an AlGaAs NW with an embedded GaAs QD. AlGaAs NWs were grown on GaAs (1 1 1)B semiinsulating substrate using an EP1203 MBE system equipped with solid sources supplying Ga and Al atoms, and an As effusion cell to produce tetramers. The Al content along the NW and within the wire cross sections was monitored by Raman spectroscopy in order to exclude possible inhomogeneities. We have found Al concentration in the range $c = 0.24$ – 0.26 .

The substrate surface was first deoxidized at 630°C . Then a 100-nm-thick GaAs buffer layer was grown at 600°C to achieve an atomically flat surface. By means of the Au effusion cell installed directly in the III–V growth chamber, an amount of gold equivalent to a 1-nm layer was deposited, without V-group flux, at 550°C to create Au droplets. Deposition was followed by a 1 min waiting time to achieve better homogeneity of the droplets, which have been used as a catalyst for the NW growth. During the subsequent NW growth, the $\text{As}_4/(\text{Ga}+\text{Al})$ flux ratio

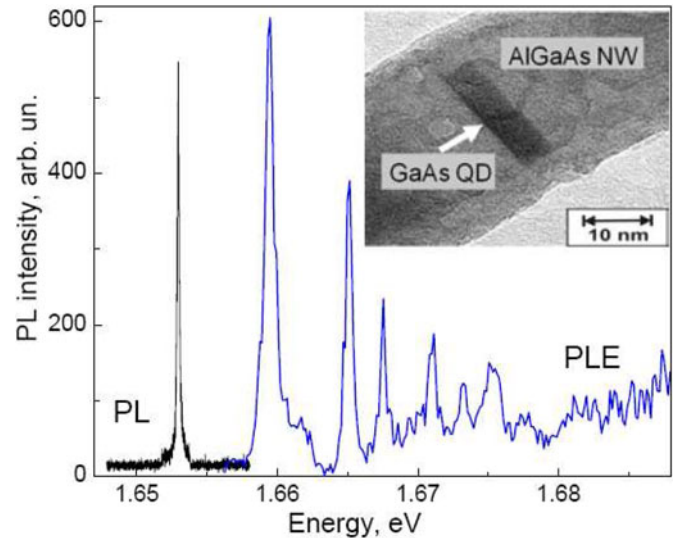


Fig. 1. PL spectrum taken from a single QD at the excitation by 533 nm laser line with intensity of 0.1 W/cm^2 . PLE spectrum taken from the same QD. Insert: TEM image of the GaAs QD in the AlGaAs NW.

was set at ≈ 1 . Growth of NWs was initiated by opening the Al, Ga, and As sources, simultaneously. The growth temperature was equal to 550°C . After 15 min, the Al source was closed for 5 s in order to form a GaAs slice in each NW. Growth of AlGaAs was then continued to produce a core-shell structure. The growth was completed with 2 min deposition of GaAs at 530°C to avoid possible oxidation of the AlGaAs shell layer. The diameter of NWs in our samples is in the range 20–50 nm. Scanning electron microscopy and transmission electron microscopy (TEM) characterizations were performed before the optical measurements.

Microspectroscopy was used to study the optical properties of individual QD inserted in NWs. The low temperature (5 K) PL of single NWs was excited by a tunable continuous wave Ti:Sa laser. We used a high numerical aperture microscope objective ($\text{NA} = 0.55$, $\times 50$) to focus the laser beam and collect the PL signal. The average power of excitation was in the μW range with a laser spot diameter lower than $1 \mu\text{m}$ allowing the extract the signal from individual NWs on as-grown samples. The PL was then dispersed by a 2 m additive double monochromator and detected by a cooled Si CCD camera. Additionally, the setup allows measure spectra with time resolution.

The TEM image of the single AlGaAs NW with a slice of GaAs is shown in the insert of Fig. 1. The dark area corresponds to the single GaAs QD. It is clearly seen that the interfaces along the axis of growth and along the radius are rather sharp. Considering cylindrical symmetry, the GaAs QD looks like a disk surrounded by the wide-gap semiconductor AlGaAs. The diameter of the NW in our samples was 25–50 nm, the length 1000 nm, and the thickness of the QD was of several monoatomic layers, i.e., 2–5 nm.

Fig. 1 shows PL spectra taken from a single QD embedded into a NW. At low excitation intensities of about 0.1 W/cm^2 a single narrow line is observed at the energy of 1.6525 eV. In the PL measurement presented here, the PL linewidth is not limited by the spectral resolution. It corresponds to an inhomogeneous

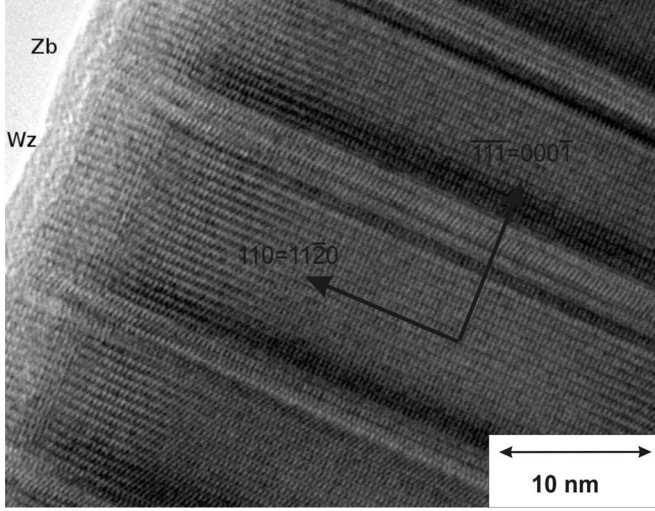


Fig. 2. TEM image of an AlGaAs NW with wurtzites and zincblende phase alternations.

broadening induced by fluctuations of a local electric field. It is natural to connect this line with the annihilation of an exciton in the single QD. This figure shows also the spectrum of PLE taken from the same dot. The distance between the absorption (PLE) lines corresponds to the “transverse” carrier quantization in the dot of 15 nm in diameter. The energy of the “longitudinal” quantization is ≈ 130 meV, which corresponds to the QD thickness of 2.5 nm. In the PLE spectrum, one can see very broad absorption lines at high energy; we connect these lines with carrier absorption in the NW itself.

In Fig. 2, a TEM image of one of our AlGaAs NW clearly shows the evidence of phase transitions from Zb to Wz crystal structures. Here, layers in which the brighter lines appear parallel to the growth direction corresponds to ABAB lattice repetitions of Wz, whereas the layers in which the bright lines appear to zigzag correspond to the ABC repetitions of the Zb phase. Interestingly, the darkest layers between the two crystal phases suggest the presence of a strain field given by a lattice mismatch between Zb and Wz AlGaAs.

III. MODELS

A. Strain Calculations

The continuum model, we have used for our calculations of the electromechanical fields has been derived following the theory in [25]. The total mechanical and electrical free energy density change dU of a piezoelectric medium can be written as [26]

$$dU = dU^{\text{mech}} + dU^{\text{elec}} = TdS + \sigma_{ik}d\varepsilon_{ik} + E_idD_i \quad (1)$$

where T , S , σ_{ik} , ε_{ik} , E_i , and D_i are the temperature, entropy, stress tensor, strain tensor, electric field, and electric displacement, respectively.

With isentropic conditions ($dS = 0$) and using crystal symmetry considerations the elastic energy for a crystal with Zb

symmetry read [27]

$$U_{Zb}^{\text{mech}} = \frac{1}{2}[C_{11,Zb}(\varepsilon_{xx}^2 + \varepsilon_{yy}^2 + \varepsilon_{zz}^2) + 2C_{12,Zb}(\varepsilon_{xx}\varepsilon_{yy} + \varepsilon_{xx}\varepsilon_{zz} + \varepsilon_{yy}\varepsilon_{zz}) + 4C_{44,Zb}(\varepsilon_{xy}^2 + \varepsilon_{xz}^2 + \varepsilon_{yz}^2)] \quad (2)$$

where $C_{ij,Zb}$ are the linearly independent stiffness constant parameters for a Zb structure.

Similarly, for a crystal with Wz symmetry we have for the elastic energy [27]

$$U_{Wz}^{\text{mech}} = \frac{1}{2}[C_{11,Wz}(\varepsilon_{xx}^2 + \varepsilon_{yy}^2) + C_{33,Wz}\varepsilon_{zz}^2 + 2C_{12,Wz}\varepsilon_{xx}\varepsilon_{yy} + 2C_{13,Wz}\varepsilon_{zz}(\varepsilon_{xx} + \varepsilon_{yy}) + 4C_{44,Wz}(\varepsilon_{xz}^2 + \varepsilon_{yz}^2) + 2(C_{11,Wz} - C_{12,Wz})\varepsilon_{xy}^2] \quad (3)$$

where $C_{ij,Wz}$ are the linearly independent stiffness constant parameters for a Wz structure.

While the stiffness parameters for Zb GaAs, AlAs, and AlGaAs alloy can be found in the literature [28], we do not have available the correspondent Wz parameters, so we have estimated them from Martin’s transformations [23], [24] using the Zb parameters

$$\begin{aligned} C_{11,Wz} &= \frac{1}{6}(3C_{11,Zb} + 3C_{12,Zb} + 6C_{44,Zb}) \\ &\quad - 3\Delta^2/(C_{11,Zb} - C_{12,Zb} + C_{44,Zb}) \\ C_{12,Wz} &= \frac{1}{6}(C_{11,Zb} + 5C_{12,Zb} - 2C_{44,Zb}) \\ &\quad + 3\Delta^2/(C_{11,Zb} - C_{12,Zb} + C_{44,Zb}) \\ C_{13,Wz} &= \frac{1}{6}(2C_{11,Zb} + 4C_{12,Zb} - 4C_{44,Zb}) \\ C_{33,Wz} &= \frac{1}{6}(2C_{11,Zb} + 4C_{12,Zb} + 8C_{44,Zb}) \\ C_{44,Wz} &= \frac{1}{6}(2C_{11,Zb} - 2C_{12,Zb} + 2C_{44,Zb}) \\ &\quad - 6\Delta^2/(C_{11,Zb} - C_{12,Zb} + 4C_{44,Zb}) \end{aligned} \quad (4)$$

where

$$\Delta \equiv \frac{\sqrt{2}}{6}(C_{11,Zb} - C_{12,Zb} - 2C_{44,Zb}). \quad (5)$$

The piezoelectric field is included directly in our fully coupled continuum model [25], and the not available Wz piezoelectric parameters have been approximated using parameters of well-known Wz materials, as GaN, AlN, and AlGaN alloy. Expressions from (1) to (5) have been used to derive the governing equations of the electromechanical fields of the crystal [25].

B. $\vec{k} \cdot \vec{p}$ Method

We have used for band structure calculations an eight-band $\vec{k} \cdot \vec{p}$ model [21], which describes electron, heavy-hole, light-hole, and spin-orbit split-off bands around the Γ point of the Brillouin zone and treats all other bands as remote bands. An

8×8 effective-mass Hamiltonian has been implemented, based on Foreman's application of Burt's exact envelope function theory to planar heterostructures [29].

The wave function of a state n with energy E_n is given by a linear combination of the eight Bloch parts weighted by the respective envelope functions,

$$\psi_n(r) = \sum_{i=1}^8 \phi_i(r) u_i(r) \quad (6)$$

where ϕ_i are the envelope function and u_i are the Bloch states at $k = 0$ [30].

The Luttinger–Kohn parameters the Zb $\vec{k} \cdot \vec{p}$ Hamiltonian ($L_1, L_2, M_1, M_2, M_3, N_1$, and N_2) have been taken from [28], while the A_i parameters in the Pikus–Bir model for Wz have been derived from the correspondent Zb materials using the cubic approximation as described in [22]

$$\begin{aligned} A_1 &= -\gamma_1 - 4\gamma_2 & A_2 &= -\gamma_1 + 2\gamma_2 & A_3 &= 6\gamma_2 \\ A_4 &= -3\gamma_2 - 1 & A_5 &= -3\gamma_3 & A_6 &= -3\sqrt{2}\gamma_3. \end{aligned} \quad (7)$$

GaAs Pikus–Bir parameters are in good agreement with the corresponding parameters given by GW calculations in [20]. For the band offset of the GaAs Wz material, we refer to [14], and we have assumed an equivalent offset for the AlAs Wz material. Results for electromechanical fields with the continuum model are included in the framework of the $\vec{k} \cdot \vec{p}$ as it is usually done via deformation potentials [31].

The complete set of parameters for the Wz materials, we have used for our simulations is given in Table I, with the same usual notation as in [28].

Optical properties are calculated in the dipole approximation, starting from the dipole matrix elements $\vec{\mu}_{nm}$, between states n and m , respectively. These are calculated from the momentum matrix elements which is represented in the k-space as [32]

$$p_{nm}^{\vec{k}} = \frac{m_0}{\hbar} \frac{\partial H_{nm}}{\partial \vec{k}}. \quad (8)$$

Finally, oscillator strengths for the optical transitions are given by [33]

$$\vec{P}_{nm} = \frac{2\pi e^2 \hbar^2}{\epsilon_0 m_0^2 V} |\hat{e} \cdot \vec{p}_{nm}|^2 \quad (9)$$

where \hat{e} is the direction unit vector of the electric field of the linearly polarized incident light, V is the quantum dot volume, e is the electron charge, and ϵ_0 is the vacuum permittivity.

C. Geometry and Structure

In our simulations, we have considered an $\text{Al}_c\text{Ga}_{1-c}\text{As}$ nanowire ($c = 0.25$) with a diameter of 40 nm and height of 50 nm, with an embedded GaAs QD with a diameter of 20 nm and an height of 5 nm. Two different cases have been studied and compared: a pure Zb case, where the whole structure is assumed to be grown in pure Zb crystal phase, and a mixed structure as shown in Fig. 3, where the GaAs QD is sandwiched by two adjacent 8-nm-high Wz layers and surrounded by a Zb AlGaAs shell. The mixed structure is completed by Zb layers at the top and at the bottom. We will refer in the following to this structure as the mixed (Mx) case.

TABLE I
PARAMETERS FOR THE Wz STRUCTURES USED IN THE SIMULATIONS

Parameters	GaAs Wz	AlAs Wz
a (nm)	0.399	0.4002
c (nm)	0.653	0.654
E_g (eV)	1.552	3.216
Δ_{cr} (eV)	0.010	-0.169
Δ_{so} (eV)	0.017	0.019
m_e^{\parallel} (eV)	0.202	0.300
m_e^{\perp} (eV)	0.206	0.320
A_1	-15.22	-7.04
A_2	-2.86	-2.12
A_3	12.36	4.92
A_4	-7.18	-3.46
A_5	-8.79	-4.26
A_6	-12.43	-6.02
VBO (eV)	0.716	1.246
a_1 (eV)	-6.8	1.0
a_2 (eV)	-8.6	-7.2
D_1 (eV)	-3.7	-17.1
D_2 (eV)	4.5	7.9
D_3 (eV)	8.2	8.8
D_4 (eV)	-4.1	-3.9
D_5 (eV)	-4.0	-3.4
D_6 (eV)	-5.5	-3.4
C_{11} (GPa)	145	141
C_{12} (GPa)	51	49
C_{13} (GPa)	38	41
C_{33} (GPa)	158	149
C_{44} (GPa)	38	40
e_{13} (C/m^2)	-0.49	-0.65
e_{33} (C/m^2)	0.81	1.50
e_{15} (C/m^2)	-0.11	-0.24

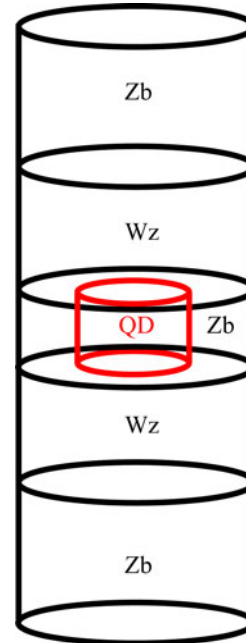


Fig. 3. Scheme of the simulated AlGaAs nanowire with the embedded GaAs quantum dot (QD) for Mx case. The different crystal phases of the correspondent layers are also indicated. All the dimensions are given in the text.

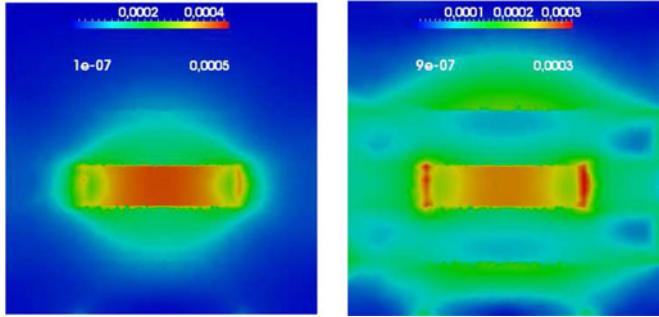


Fig. 4. (Left) Magnitude of the absolute value of strain field for a pure Zb structure and (right) for the Mx structure.

IV. RESULTS

A. Electromechanical Fields

The electromechanical fields (strain and piezoelectric fields) are evaluated as described in Section III-A. In Fig. 4, we plot the magnitude of the absolute value of the strain field for the pure Zb and the Mx structures, respectively.

It is interesting to notice that in the Mx case, besides the usual strain field inside and in the proximity of the QD, given by the lattice mismatch between the two materials, we can observe a weaker strain field at the interfaces between the two crystal phases of AlGaAs. This field is also observed in the TEM image shown in Fig. 2. Despite its weakness, which was indeed expected from the small lattice mismatch between the GaAs and the $\text{Al}_c\text{Ga}_{1-c}\text{As}$ ($c = 0.25$) and the even smaller crystal mismatch between Zb- and Wz- AlGaAs, the strain field is nonzero practically everywhere in the nanowire. This also affects the electric properties of the structure.

The electric field originating from the piezoelectric effect in the Mx case is relatively strong and presents an unusual shape, different from the typical results obtained for Zb QDs. This can be observed in Fig. 5, showing the z component of the electric field for both Zb and Mx structures.

Instead of the usual quadrupole shape obtained for Zb QDs, the Mx case gives a Wz-like shape of the electric field close and inside the dot, with its typical dipole characteristics, and opposite signs inside and just outside of the top and the bottom of the dot. This occurs even though the central volume of the column is in a pure Zb crystal phase and owes to the stronger magnitude of the piezoelectric effect induced by the Wz layers, which leads to a stronger electric field. A stronger magnitude of the piezoelectric effect in Wz heterostructures compared to Zb heterostructures has been already reported in the literature [27].

B. Results for Confined States

The quantum confinement in the QD is mainly given by the band offset between the two materials and between the two different crystal structures of the AlGaAs in the Mx case, since the impact of the observed strain fields on the confinement via the deformation potentials [31] is not particularly relevant. In Fig. 6, we plot the conduction E_c and valence E_v band along the z direction for Zb and Mx structures.

The usual case of a Zb QD embedded in a Zb matrix has been considered as a useful comparison in order to better understand

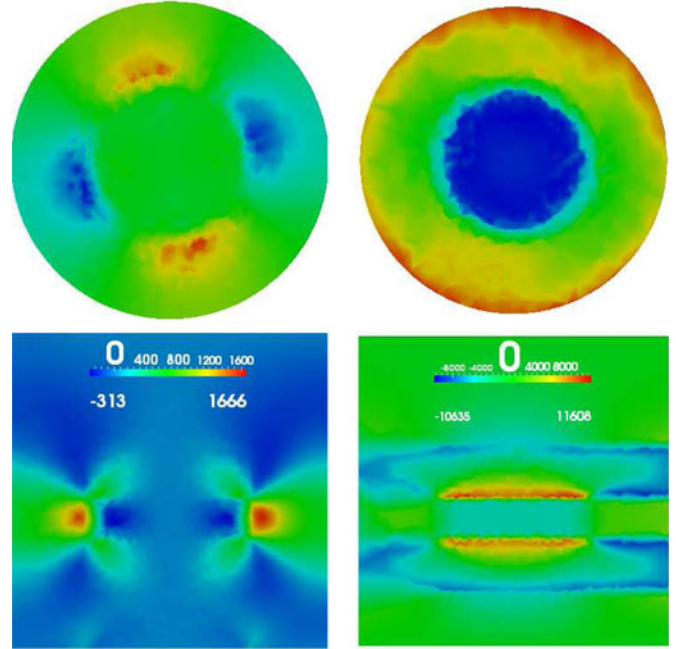


Fig. 5. (Top) z component of the electric field in the xy plane in the middle of the QD and (bottom) in the xz planes, respectively. (Left column) Zb structure and (right column) Mx structure. All values in G Volt/m.

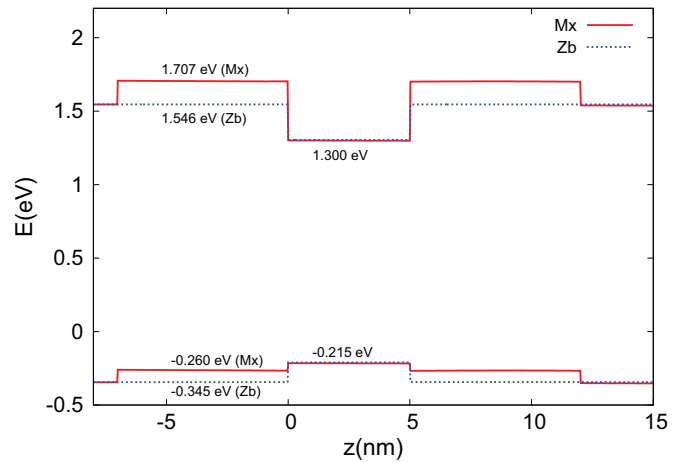


Fig. 6. (Top part) Conduction and (bottom part) valence band along the z direction for both the Zb and the Mx cases. The energy is expressed in eV, where the 0 is given by the Fermi level.

the results for the energy levels. For the Mx conduction band, the well of the QD is surrounded by the energetically higher barrier of the Wz layers, higher as compared to the lower potentials of the Zb AlGaAs. This results in an increased quantum confinement for the electron states. On the other hand, the hole bands of the Mx structure exhibit a sort of double well with the potential profile of the QD and the two adjacent Wz layers acting as a second wider well, that can contain several confined states. The form of the potential has a notable impact on the hole wave functions.

In Fig. 7, we plot all the confined states for the electrons and the holes for both Zb and Mx situations. All states are doubly degenerate for spin inversion due to time reversal symmetry.

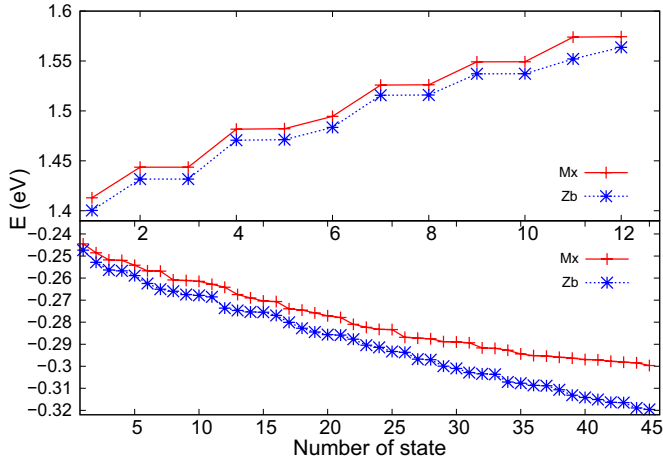


Fig. 7. (Top) Calculated states for electrons and (bottom) holes. The x scales enumerates the number of the correspondent state (different scale for electrons and holes), while the energy in the y -axis is referred to the Fermi level as in Fig. 6.

As far as electron states are concerned, the main difference we observe between the Zb case and the Mx case is a higher degree of quantum confinement in the latter, which slightly increases the energy levels and gives rise to two further confined states, i.e., states 11 and 12 are delocalized in the Zb model, while confined within the QD in the Mx case.

The shape and the symmetry of the electron wave functions do not significantly differ between the two models, implying that they are mainly dependent on the Zb crystal structure of the QD, and are barely affected by the electric field and its symmetries. However, the actual lack of knowledge of the real values of piezoelectric coefficients for the Wz phase of these materials makes uncertain the impact of the electric field on the symmetry of the wave functions.

The higher electron states are completely delocalized in the Zb layers adjacent to the Wz layers. These states are not optically active, since they have almost zero overlap with the hole wave functions confined in the QD.

The situation for the hole states is notably different and quite interesting. Comparing the curves plotted in the bottom part of Fig. 7, it is clearly possible to see that, while the first confined states of the two models are very close in energy (also showing a similar trend), higher energy states (in absolute value) display different trends. The states of the Mx model are systematically lower in energy. The onset of this change corresponds to states that start to delocalize in the Wz layers, adjacent to the QD. The increased available volume explains their lower energy compared to the case of a pure Zb structure. This is confirmed by the contour plots of the probability density which we show in Fig. 8. Here, we present a slice of the xz plane, with $x = 30$ nm and $z = 40$ nm, showing basically the center of the nanowire with the dot and the two adjacent Wz layers.

Fig. 8 (left) shows the probability density of the holes ground state, which, as expected, is completely confined in the QD. Fig. 8 (right) shows the probability density of the hole state number 32, according the bottom y labeling of Fig. 7. This state is mainly confined in the Wz layers. A similar situation, with states confined in the volume formed by the QD and the two

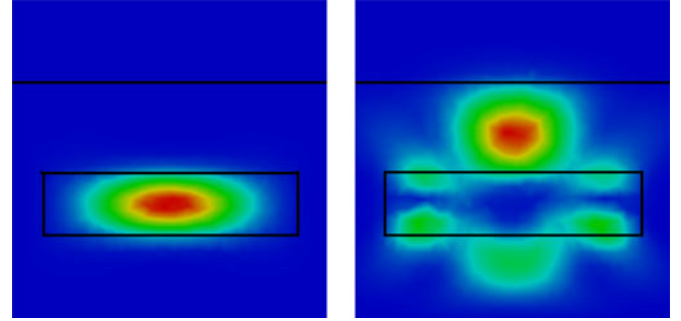


Fig. 8. (Left) Holes ground state and (right) holes state number 32 according the bottom y labeling of Fig. 7 in xz plane ($x = 30$ nm and $z = 40$ nm). (Below) Continuous lines indicate the edges of the QD and (top) edge between the Wz and the Zb phase.

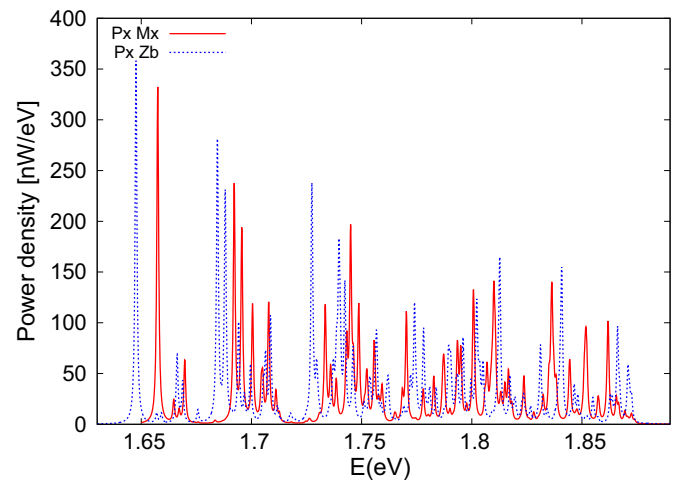


Fig. 9. Oscillator strengths in x directions for the two models.

adjacent Wz layers, is observable for a considerable number of the higher energy hole states. All these states are optically active, since they have a nonzero overlap with the electron states confined in the dot.

C. Oscillator Strengths Results

We finally present results for the oscillator strengths, according dipole approximation. In Fig. 9, we show the optical transitions. Despite some resemblances in the distributions of the peaks, we can notice an effect which confirms what we have discussed in the previous section. We observe a blue shift of the lowest transitions of the Wz instance, namely for the ground state–ground state transition and the transitions between the more confined energy levels. This is clearly due to the higher energy of the electrons in the Mx case. But, on the other hand, for the peaks at higher energy, we notice a red shift of the lines correspondent to the Mx models, due to the difference in energy between the less confined hole states, up to 20 meV as observable in Fig. 7.

Finally, in Fig. 10, the lowest range of the spectrum is compared with the positions of three peaks given by experimental results from a specific NW sample with approximately the same dimensions of our model.

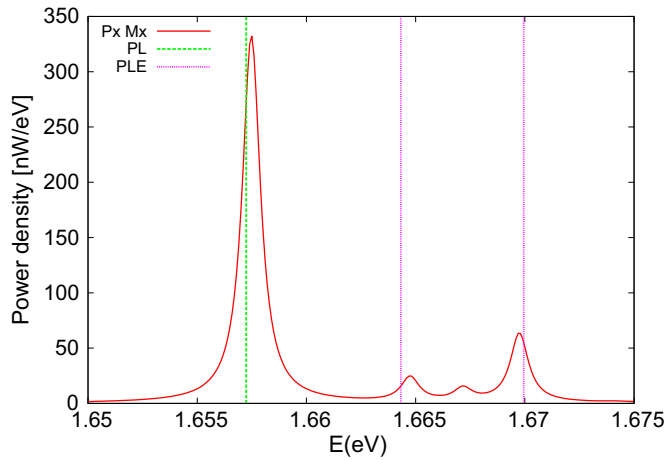


Fig. 10. Oscillator strengths in x directions for the Mx model compared with the positions of experimental transition results: PL for the first transition, PLE for the second and third ones.

Here, the peak correspondent to the lowest transition, namely the ground state–ground state transition, has been measured by a PL experiment, while the other two positions we show are given by a PLE data set from the same sample. Although our Mx model cannot be completely validated due to the fluctuation of measurement data from different samples, the agreement for this particular sample is very good.

V. CONCLUSION

We have presented numerical simulations for polymorph Wz-Zb cylindrical AlGaAs NW with an embedded GaAs QD. First, the connection with experimental structures has been shown, and consequently suitable continuum elastic and eight-band $\vec{k} \cdot \vec{p}$ models have been derived. All the necessary numerical parameters have been determined by appropriate approximations, where not available in the previous literature.

The results for the strain fields are in a good agreement with the experimental data, showing, besides the usual field given by the lattice mismatch between different material, a nonzero field at the interfaces between the two crystal phase of AlGaAs.

The analysis of the confined energy levels, wave functions, and optical transitions clearly show the differences between an uniform crystal phase and a polymorph heterostructure. The comparison of numerical results and experimental spectra for optical transitions comfort the validity of our polymorph numerical model.

REFERENCES

- [1] D. Leonard, K. Pond, and P. M. Petroff, "Critical layer thickness for self-assembled InAs islands on GaAs," *Phys. Rev. B*, vol. 50, p. 11687, 1994.
- [2] J.-Y. Marzin, J.-M. Gerard, A. Izrael, D. Barrier, and G. Bastard, "Photoluminescence of Single InAs quantum dots obtained by self-organized growth on GaAs," *Phys. Rev. Lett.*, vol. 73, p. 716, 1994.
- [3] T. Bryllert, L. E. Wernersson, T. Lowgren, and L. Samuelson, "Vertical wrap-gated nanowire transistors," *Nanotechnology*, vol. 17, p. S227, 2006.
- [4] S. Gratecak, F. Qian, Y. Li, H. G. Park, and C. M. Lieber, "GaN nanowire lasers with low lasing thresholds," *Appl. Phys. Lett.*, vol. 87, p. 173111, 2005.
- [5] V. G. Dubrovskii, G. E. Cirlin, I. P. Soshnikov, A. A. Tonkikh, N. V. Sibirev, Yu. B. Samsonenko, and V. M. Ustinov, "Diffusion-induced

- growth of GaAs nanowhiskers during molecular beam epitaxy: Theory and experiment," *Phys. Rev. B*, vol. 71, p. 205325, 2005.
- [6] J. C. Harmand, G. Patriarche, N. Péré-Laperne, M.-N. Mérat-Combes, L. Travers, and F. Glas, "Analysis of vapor-liquid-solid mechanism in Au-assisted GaAs nanowire growth," *Appl. Phys. Lett.*, vol. 87, p. 203101, 2005.
- [7] M. C. Plante and R. R. La Pierre, "Growth mechanisms of GaAs nanowires by gas source molecular beam epitaxy," *J. Cryst. Growth*, vol. 286, no. 2, p. 394, 2006.
- [8] V. G. Dubrovskii, N. V. Sibirev, G. E. Cirlin, J. C. Harmand, and V. M. Ustinov, "Theoretical analysis of the vapor-liquid-solid mechanism of nanowire growth during molecular beam epitaxy," *Phys. Rev. E*, vol. 73, p. 021603, 2006.
- [9] V. G. Dubrovskii, N. V. Sibirev, G. E. Cirlin, A. D. Bouravleuv, Yu. B. Samsonenko, D. L. Dheeraj, H. L. Zhou, C. Sartet, J. C. Harmand, G. Patriarche, and F. Glas, "Role of nonlinear effects in nanowire growth and crystal phase," *Phys. Rev. B*, vol. 80, p. 205305, 2009.
- [10] V. N. Kats, V. P. Kochereshko, A. V. Platonov, T. V. Chizhova, G. E. Cirlin, A. D. Bouravleuv, Yu. B. Samsonenko, I. P. Soshnikov, E. V. Ubyivovk, J. Bleuse, and H. Mariette, "Optical study of GaAs quantum dots embedded into AlGaAs nanowires," *Semicond. Sci. Technol.*, vol. 27, p. 015009, 2012.
- [11] O. Demichel, M. Heiss, J. Bleuse, H. Mariette, and A. Fontcuberta i Morral, "Impact of surfaces on the optical properties of GaAs nanowires," *Appl. Phys. Lett.*, vol. 97, p. 201907, 2010.
- [12] G. Sallen, A. Tribu, T. Aichele, R. André, L. Besombes, C. Bougerol, M. Richard, S. Tatarenko, K. Kheng, and J.-Ph. Poizat, "Subnanosecond spectral diffusion of a single quantum dot in a nanowire," *Phys. Rev. B*, vol. 84, p. 041405, 2011.
- [13] J. Bleuse, J. Claudon, M. Creasey, N. S. Malik, J.-M. Gérard, I. Maksymov, J.-P. Hugonin, and P. Lalanne, "Inhibition, enhancement, and control of spontaneous emission in photonic nanowires," *Phys. Rev. Lett.*, vol. 106, p. 103601, 2011.
- [14] D. Spirkoska, J. Arbiol, A. Gustafsson, S. Conesa-Boj, F. Glas, I. Zardo, M. Heigoldt, M. H. Gass, A. L. Bleloch, S. Estrade, M. Kaniber, J. Rossler, F. Peiro, J. R. Morante, G. Abstreiter, L. Samuelson, and A. Fontcuberta i Morral, "Structural and optical properties of high quality zinc-blende/wurtzite GaAs nanowire heterostructures," *Phys. Rev. B*, vol. 80, p. 245325, 2009.
- [15] W. P. Harrison, *Electronic Structure and the Properties of Solids*. New York, USA: Dover Publications, 1989.
- [16] J. M. Luttinger and W. Kohn, "Motion of electrons and holes in perturbed periodic fields," *Phys. Rev.*, vol. 97, pp. 869–883, 1955.
- [17] Z. Zanolli, F. Fuchs, J. Furthmüller, U. von Barth, and F. Bechstedt, "Model GW band structure of InAs and GaAs in the wurtzite phase," *Phys. Rev. B*, vol. 75, p. 245121, 2007.
- [18] A. De and C. E. Pryor, "Predicted band structures of III-V semiconductors in the wurtzite phase," *Phys. Rev. B*, vol. 81, p. 155210, 2010.
- [19] J.-M. Jancu, K. Gauthron, L. Largeau, G. Patriarche, J.-C. Harmand, and P. Voisin, "Type II heterostructures formed by zinc-blende inclusions in InP and GaAs wurtzite nanowires," *Appl. Phys. Lett.*, vol. 97, p. 041910, 2010.
- [20] T. Cheiwchanchamnangij and W. R. L. Lambrecht, "Band structure parameters of wurtzite and zinc-blende GaAs under strain in the GW approximation," *Phys. Rev. B*, vol. 84, p. 035203, 2011.
- [21] L. C. Lew Yan Voon and M. Willatzen, *The $K-p$ Method: Electronic Properties of Semiconductors*. New York, USA: Springer-Verlag, 2009.
- [22] S. L. Chuang and C. S. Chang, "k-p method for strained wurtzite semiconductors," *Phys. Rev. B*, vol. 54, p. 2491, 1996.
- [23] R. M. Martin, "Relation between elastic tensors of wurtzite and zinc-blende structure materials," *Phys. Rev. B*, vol. 6, p. 4546, 1972.
- [24] A. F. Wright, "Elastic properties of zinc-blende and wurtzite AlN, GaN, and InN," *J. Appl. Phys.*, vol. 82, p. 6, 1997.
- [25] D. Baretin, S. Madsen, B. Lassen, and M. Willatzen, "Computational methods for electromechanical fields in self-assembled quantum dots," *Commun. Comput. Phys.*, vol. 11, pp. 797–830, 2012.
- [26] L. D. Landau and E. M. Lifshitz, *Theory of Elasticity*, Course of Theoretical Physics, vol. 7, Pergamon Press, 1970.
- [27] V. A. Fonoberov and A. A. Balandin, "Excitonic properties of strained wurtzite and zinc-blende GaN/Al_xGa_{1-x}N quantum dots," *J. Appl. Phys.*, vol. 94, p. 7178, 2003.
- [28] I. Vurgaftman, J. R. Meyer, and L. R. Ram-Mohan, "Band parameters for III-V compound semiconductors and their alloys," *J. Appl. Phys.*, vol. 89, p. 5815, 2001.

- [29] B. A. Foreman, "Effective-mass Hamiltonian and boundary conditions for the valence bands of semiconductor microstructures," *Phys. Rev. B*, vol. 48, pp. 4964–4976, 1993.
- [30] E. P. Pokatilov, V. A. Fonoberov, V. M. Fomin, and J. T. Devreese, "Development of an eight-band theory for quantum dot heterostructures," *Phys. Rev. B*, vol. 64, p. 245328, 2001.
- [31] G. L. Bir and G. E. Pikus, *Symmetry and Strain-Induced Effects in Semiconductors*. New York: Wiley, vol. 295, 1974.
- [32] L. C. Lew Yan Voon and L. R. Ram-Mohan, "Tight-binding representation of the optical matrix elements: Theory and applications," *Phys. Rev. B*, vol. 47, p. 15500, 1993.
- [33] O. Stier, M. Grundmann, and D. Bimberg, "Electronic and optical properties of strained quantum dots modeled by 8-band kp theory," *Phys. Rev. B*, vol. 59, p. 5688, 1999.



Daniele Baretin received the Master degree in physics from the University of Rome "La Sapienza," Rome, Italy, and the Ph.D. degree in applied mathematical models from the University of Southern Denmark.

Since 2011, he has been a Postdoctoral Researcher with the Department of Electronic Engineering of the University of Rome "Tor Vergata," Rome. His research interests include the study of optoelectronic properties of nanostructures, optimization of organic electronic devices, and the study of complex systems

in statistical mechanics.



Alexei V. Platonov received the Master degree in physics from the St.Petersburg State Polytechnical University, St.Petersburg, Russia in 1996, and the Ph.D. degree in Physics and Mathematics from Ioffe Physical Technical Institute RAS, St.Petersburg, in 1999.

He has been a Senior Researcher at the laboratory of the solid-state spectroscopy, Ioffe Physical Technical Institute RAS, since 2004. His research interest includes the optical properties of the semiconductor heterostructures.



Alessandro Pecchia received the degree in physics from the University of Trieste, Trieste, Italy, in 1998 and the Ph.D. degree from the University of Leeds, Leeds, U.K., in 2002.

He has been a CNR Researcher since 2005, working also in close collaboration with the Department of Electronic Engineering of the University of Rome "Tor Vergata," Rome, Italy. His research interest includes transport properties of nanostructures and on molecular electronics.



Vladimir N. Kats received the Master degree in physics from the St.Petersburg State University, St.Petersburg, Russia, in 2008.

He is a Junior Researcher at the laboratory of Optics of Spin, St.Petersburg State University since 2012. He is a Junior Researcher at the laboratory of Solid-State Spectroscopy, Ioffe Physical Technical Institute RAS, St.Petersburg, Russia since 2012. His research interest includes the study of semiconductor nanostructures optical properties.



George E. Cirlin received the B.S. and M.S. degrees from Leningrad Electrotechnical Institute, St. Petersburg, Russia, and the Ph.D. and D.Sc. degrees from the Institute for Analytical Instrumentation RAS, St. Petersburg, in 1985, 1987, 1991, and 2001, respectively, all in semiconductor physics.

He is the Head of the Laboratory of Epitaxial Nanotechnologies, Academic University RAS, and Leading Research Scientist at Ioffe Institute, St. Petersburg, Russia. His research interest has been in the areas of growth and investigation of semiconductor nanostructures. He has authored about 350 papers in leading journals and conferences and two international patents. His current research interests include nanowire and quantum dots physics and technology.



Iliya P. Soshnikov received the Graduation degree from the Department of Physics, State University, St. Petersburg, Russia, in 1988, and the Ph.D. degree in solid state physics from State Technical University, St. Petersburg, in 1997.

Since 1997, he has been with the Laboratory of Physics of Semiconductor Heterostructures, A.F.Ioffe Physico-Technical Institute, St. Petersburg. His research interests include structural investigation of semiconductor heterostructures and postgrowth treatment methods for semiconductor

heterostructure.



Alexei D. Bouravlev received the Master's degree in physics from the St. Petersburg State Polytechnical University, St. Petersburg, Russia, in 1999, and the Ph.D. degree in physics and mathematics from Ioffe Physical Technical Institute RAS, St. Petersburg, in 2002.

Since 2008, he has been a Senior Researcher at the laboratory of physics of elementary surface structures, Ioffe Physical Technical Institute RAS. His research interests include the study of the growth processes of semiconductor nanostructures and their

properties.



Lucien Besombes was born in 1974. He received the Ph.D. degree from the University Joseph-Fourier, Grenoble, France, in 2001.

After a two years postdoctoral stay in the Quantum Optoelectronics Group, University of Southampton, Southampton, U.K., where he developed optical coherent control experiments on quantum dots, he joined in October 2003 the Laboratoire de Spectrométrie Physique, University Joseph Fourier to start the study of the spin properties of charged and magnetic II–VI quantum dots. In 2008, he joined Neel Institute, CNRS, Grenoble, where he developed experiments for the optical control of individual spins in semiconductor quantum dots. His current research interest includes the optical coherent control of individual spins and the control of the interaction between localized spins in semiconductor nanostructures.



Henri Mariette received the the Graduation degree from the French Engineering School ESPCI-Paristec, Paris, France, and received the Ph.D. degree in physics from the University of Paris in 1981.

After postdoctoral years in Max Planck Institut (Stuttgart) and IBM (San José and Yorktown-Heights), he became a Centre National de la Recherche Scientifique Researcher and joined the Atomic Energy Commissariat and the National Center for the Scientific Research Group "Nanophysique et Semiconducteurs", Grenoble, France. His research interests include the study of epitaxial growth of various semiconductor nanostructures, exhibiting specific properties: particularly photonic source with quantum dots, diluted magnetic semiconductors for spintronic, and new bandgap engineering for photovoltaics conversion.



Matthias Auf der Maur (M'06) received the Dipl. El.-Ing. degree from the Swiss Federal Institute of Technology, Zurich, Switzerland, in 2003, and the Ph.D. degree from the University of Rome "Tor Vergata," in 2008.

He is currently a Researcher with the Department of Electronic Engineering, the University of Rome Tor Vergata. His research interests include electronic transport and optical properties of nanostructured devices and implementation of multiscale/multiphysics simulation models.



Aldo Di Carlo (M'01) received the Laurea degree in physics (*cum laude*) from the University of Rome La Sapienza, Rome, Italy, and the Ph.D. degree from the Technical University of Munich, Munich, Germany.

In 1996, he became a Research Assistant in the Department of Electronic Engineering, University of Rome "Tor Vergata," Rome, where he has been an Associate Professor, since November 2001, and the Coordinator of the Center for Hybrid and Organic Solar Energy. His current research interests include the

study of electronic and optical properties of nanostructured devices, analysis, and optimization and fabrication of organic electronic devices, charge transport in nanostructured devices, high electron mobility transistors, organic thin-film transistors, molecular devices, and carbon nanotube-FETs.